J Mater Sci: Mater Med (2007) 18:1009–1016
DOI 10.1007/s10856-006-0114-x

Calcium phosphates formation on $CaTiO_3$ coated titanium

Naofumi Ohtsu · Kenji Sato · Kesami Saito · Katsuhiko Asami · Takao Hanawa

Received: 9 May 2005 / Accepted: 27 January 2006 / Published online: 23 January 2007

Abstract In this study, performance of calcium phosphate formation of $CaTiO_3$ coating film on Ti in Hanks' balanced saline solution (HBSS) was investigated. $CaTiO_3$ thin films with a thickness of 50 nm were deposited on Ti using radiofrequency (RF) magnetron sputtering. The temperature of Ti substrate was adjusted to room temperature (RT) and 873 K. Thereafter, the specimens deposited at RT were annealed at 873 K in air for 7.2 ks. The films were characterized by grazing incident angle X-ray diffractometry (GI-XRD) and X-ray photoelectron spectroscopy (XPS). After immersion in HBSS for 60 d, on $CaTiO_3$ coated Ti, the formation of hydroxyapatite (HAP) was observed. Furthermore, HAP layer formed was thicker on the specimen on which $CaTiO_3$ film was deposited at RT and annealed than that prepared at 873 K. The major difference between both specimens was the chemical properties of the outermost surface. In summary, $CaTiO_3$ thin film deposited at RT and followed by annealing at 873 K for 7.2 ks in air enhances calcium phosphate formation ability on Ti.

Introduction

Titanium and its alloys have been widely used as biomedical and dental materials because of their excellent biocompatibility [1] and good mechanical properties [2]. However, it takes long time for these materials to bond directly to living bone. Improvement of bone-conductivity of these materials is demanded from biomedical field such as orthopedics and dentistry. In order to enhance the ability of these materials, various surface modification techniques have been attempted. Most of these techniques are physical coating processes with foreign calcium phosphate ceramic materials with high bone-conductivity, such as hydroxyapatite (HAP; $Ca_{10}(PO_4)_6(OH)_2$) and tricalcium phosphate (TCP; $Ca_3(PO_4)_2$). Ceramic coatings due to various deposition techniques, e.g. electrophoretic deposition [3], radiofrequency sputtering [4] and pulsed laser deposition [5], are investigated, and HAP coating with plasma spraying on Ti practically used for dental implants. However, various problems with HAP spray-coated Ti are pointed out by dentists. In particular, fragility of the coated HAP film itself and poor bonding strength between the film and substrate material are serious problems because they result in cracking of the coated film and at the interface during the clinical service [6]. Also, dissolution of the film during implantation is a serious problem because abrupt increase of Ca concentration in living body may induces inflammation.

Recently, bone-conductivity of Ti using implantation of Ca ions at 18 kV is accelerated [7]. It was also reported that the implanted Ca forms unequilibrium $CaTiO_3$ in the modified surface and it promotes the formation of calcium phosphates in the living body [8, 9]. Therefore, it is expected that the bone-conductivity of Ti surface will be enhanced by coating with such a $CaTiO_3$ film. One of the simplest methods to coat $CaTiO_3$ thin layer to Ti-base materials will be the sputter deposition of $CaTiO_3$. On the other hand, the

N. Ohtsu (✉) · K. Sato · K. Saito · K. Asami
Institute for Material Research, Tohoku University,
2-1-1 Katahira, Aoba-ku, Sendai 980-8577 Miyagi, Japan
e-mail: nohtsu@imr.edu

N. Ohtsu · T. Hanawa
Institute of Biomaterials and Bioengineering, Tokyo Medical and Dental University, Tokyo 101-0062, Japan

minimum thickness of the $CaTiO_3$ film for the formation of calcium phosphates will be about the same with the depth of the modified surface by Ca-ions implantation. It is known that the modified depth by Ca^+ implantation to Ti at 18 kV is about 30 nm, which is about 1/1000 compared with that of the HAP film coated with plasma splaying. Generally, mechanical properties of thin film are improved by decreasing its thickness because of dispersion of stress. Consequently, surface modification by coating with $CaTiO_3$ thin film would be better alternative of a thick HAP coating.

In this study, performance of calcium phosphate formation on $CaTiO_3$ thin film deposited with radio-frequency (RF) magnetron sputtering was investigated by immersion in simulated body fluids (SBF). In general, materials which form calcium phosphates rapidly by immersion in SBF have a good bone-conductivity. In addition, we also discussed the $CaTiO_3$ film properties required to form calcium phosphate efficiently on the basis of the characterization of $CaTiO_3$ film.

Experimental procedure

Deposition of $CaTiO_3$ film on Ti

Commercially available pure Ti (cpTi) grade 2 (ISO 5832-2) with a disk shape (ϕ8 mm × t1 mm) was mechanically polished with SiC paper (#1500) to obtain a rough surface. $CaTiO_3$ films were deposited on cpTi substrate using RF magnetron sputtering with $CaTiO_3$ target in Ar gas flow. The background pressure of deposition chamber was about 10^{-7} Pa. The thickness of deposited films was estimated from the monitored sputtering rate of $CaTiO_3$ film and adjusted to about 50 nm. Sputtering power was fixed to 200 W. The $CaTiO_3$ thin film with low crystallinity dissolves rapidly in the SBF [10]. Therefore, we conducted two types of heat treatments to the film to increase the crystallinity and to prevent an abrupt dissolution: (1) the specimens were prepared at room temperature (RT), followed by annealing at 873 K for 7.2 ks in air (H1), and (2) the temperature of substrate was adjusted to 873 K during deposition (H2). For comparison, some specimens were prepared at RT but did not heat-treated. Specimen preparation conditions are summarized in Table 1.

Characterization of the $CaTiO_3$ films

Grazing incident angle X-ray diffractmetry (GI-XRD) was conducted with a step-scanning mode at 0.1 deg/min and a X-ray incident angle of 1 degree against the specimen surface (Rotaflex RU-200B, Rigaku, Japan).

X-ray photoelectron spectroscopy (XPS) was carried out in a pressure of about 10^{-8} Pa. Photoelectrons were excited by Al Kα radiation ($h\nu$ = 1486.6 eV) of a monochromatized X-ray source (SSX-100, Surface Science Inc, USA). In order to correct the electron-energy shift caused by charging effect, Au thin film with about 0.5-nm thickness was deposited on all specimens and all spectra were adjusted by taking the Au $4f_{7/2}$ peak position from the Au thin film as 84.0 eV. The photoionization cross-sections of the Ti $2p_{3/2}$, Ca $2p_{3/2}$ and O 1s peaks relative to that of C 1s peak used for quantification from the integrated intensities were 5.22, 3.35 and 2.93 [11], respectively.

Evaluation of calcium phosphate formation

Hanks' balanced saline solution (HBSS) as a SBF was employed to evaluate the performance of calcium phosphate formation. The ion concentrations of the HBSS and human blood plasma are compared in Table 2. The HBSS was prepared by dissolving reagent-grade $CaCl_2$, KH_2PO_4 3H2O, KCl, NaCl, $MgSO_4$ $7H_2O$, $NaHCO_3$, and Na_2HPO_4 (Nacalai Tesque, Inc) in deionized water (Millipore). Five each specimens prepared at RT, H1 and H2 were immersed in 12.2 mL of the HBSS at 310 K for 30, 45 and 60 d. For comparison, five cpTi, which was polished by SiC paper (#1500), were also immersed. Avoiding Si contamination eluted from the vessels [12], specimens were immersed in the vessels made of perfluoroalkoxy fluoroplastic (Tefron©PFA) and the vessel was completely sealed. The pH value of HBSS was adjusted to

Table 1 Specimen preparation conditions

Symbol	Sputtering conditions			Treatment after deposition
	Sputtering power	Thickness of $CaTiO_3$ film	Temperature of substrate	
RT	200 W	50 nm	Room temperature	No
H1	200 W	50 nm	Room temperature	Keep at 873 K for 7.2 ks. in air
H2	200 W	50 nm	873 K	No

Table 2 Ion concentrations of Hanks' balanced saline solution (HBSS) and human blood plasma

	Concentration (mol l^{-1})	
	HBSS	Blood plasma
Na^+	1.42×10^{-1}	1.42×10^{-1}
K^+	5.81×10^{-3}	5.00×10^{-3}
Mg^+	8.11×10^{-4}	1.50×10^{-3}
Ca^{2+}	1.26×10^{-3}	2.50×10^{-3}
Cl^-	1.45×10^{-1}	1.03×10^{-1}
HPO_4^{2-}	7.78×10^{-4}	1.00×10^{-3}
SO_4^{2-}	8.11×10^{-4}	1.50×10^{-3}
CO_3^{2-}	4.17×10^{-3}	2.7×10^{-2}

7.4 by the addition of dropwise HCl solution twice a week. After the allotted immersion periods, the specimens were retrieved from the HBSS, gently rinsed with distilled water, and dried in a convection oven at 313 K.

The formation of the calcium phosphate was examined using GI-XRD, scanning electron microscopy (SEM) and electron probe micro-analysis (EPMA; JXA-8621MX, JEOL Inc, Japan) equipped with wavelength dispersive X-ray spectrometory (WDS) and energy dispersive X-ray analysis (EDX). The acceleration voltage of SEM and EPMA was 10 kV. The thickness of the calcium phosphate layer was determined by the observation of the cross section view of specimens using SEM when calcium phosphate layer was sufficiently thick.

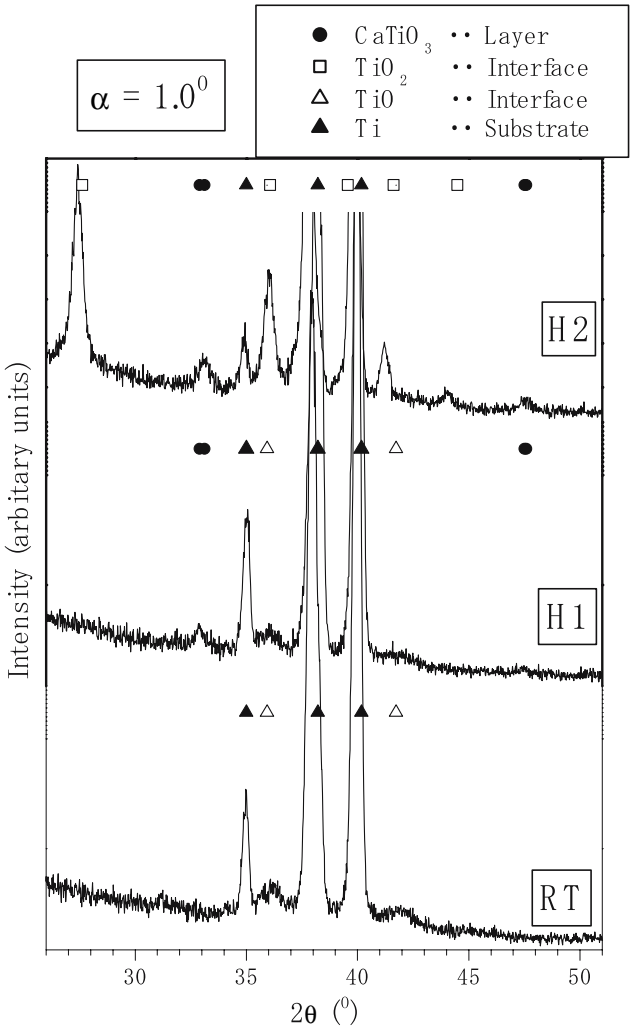

Fig. 1 GI-XRD patterns of RT, H1 and H2 specimens

Results and discussion

Characteristics of $CaTiO_3$ films before immersion

In order to utilize the surface treated cpTi and Ti-alloys in medicine and dentistry, they should be chemically stable and safe for the human body. Thus, one of the important factors for this purpose is the crystallinity of the $CaTiO_3$ film. Figure 1 shows GI-XRD patterns of the specimens before immersion. Since effective depth of GI-XRD analysis is larger than the thickness of the $CaTiO_3$ films, the GI-XRD pattern includes not only peaks from the deposited film but also those from the interface and Ti substrate. Thus, hongquiite-type TiO observed in RT and H2, and rutile type TiO_2 observed in H1 specimen were originated from the layer formed between the film and substrate. These Ti oxide layer should be formed by oxidation at the process of specimen preparation. In RT specimen, the crystallized $CaTiO_3$ was not observed. However, in both H1 and H2 specimens, perovskite-type $CaTiO_3$ was observed. These results indicate that heating at a high temperature such as 873 K is needed for the deposited $CaTiO_3$ thin film to crystallize. This crystallization temperature of $CaTiO_3$ film agrees with that of $CaTiO_3$ film prepared by sol–gel method [13].

XPS peaks of Ca 2p, Ti 2p and O 1s obtained from all specimens are shown in Fig. 2. The shape of Ca 2p peaks of RT specimen is almost symmetry, but those of H1 and H2 specimens are asymmetry and spread to higher energy side. This asymmetry is explained by the two pairs of overlapped peaks as shown in Fig. 2(a). These spectra shapes of Ca 2p and Ti 2p are similar to those of $CaTiO_3$ single-crystal [14]. The O 1s peaks of all specimens were deconvoluted into three peaks originated from anhydrous oxide (O^{2-}), hydroxyl group (OH^-) and adsorbed water (H_2O). The results are shown in Fig. 2(c). The inserted values of $\{[O^{2-}]/([OH^-] + [H_2O])\}$ to Fig. 2 are the concentration

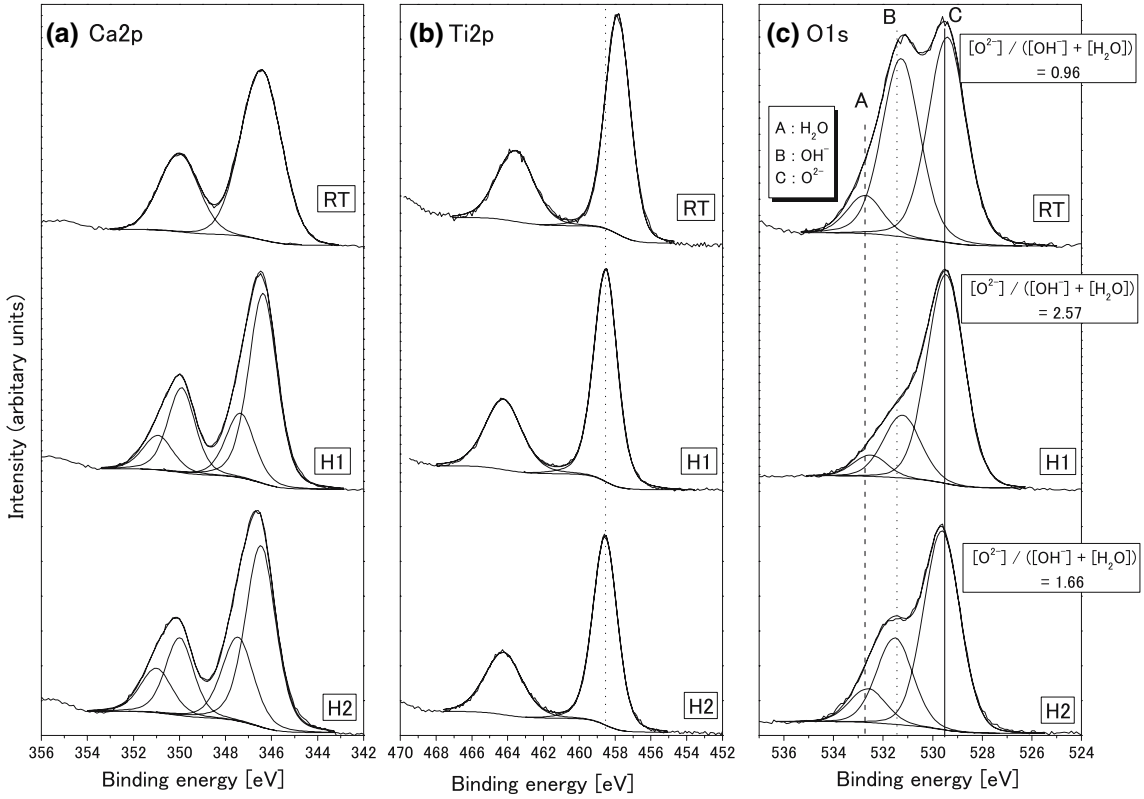

Fig. 2 XPS spectra of Ca 2p, Ti 2p and O 1s obtained from RT, H1 and H2 specimens. Binding energy values were corrected by using Au $4f_{7/2}$ = 84.0 eV. The inserted values of {$[O^{2-}]$/$[OH^-]$ + $[H_2O]$} are the concentration (at%) ratios calculated from the integrated intensities of O1s peaks

(at%) ratios calculated from the integrated intensities of O1s peaks. The {$[O^{2-}]$/($[OH^-]$ + $[H_2O]$)} concentration (at%) ratios at outermost surface increases in order of RT, H2 and H1 specimens.

The binding energies of Ca $2p_{3/2}$, Ti $2p_{3/2}$, and O 1s energy region peaks are summarized in Table 3. Table 3 also contains the binding energies obtained from $CaTiO_3$, TiO_2 and CaO by a previous study [8]. The binding energies of Ca $2p_{3/2}$ level of all specimens are the almost same as those of $CaTiO_3$. The binding energies of Ti $2p_{3/2}$ level in H1 and H2 specimens are almost the same as that of $CaTiO_3$. The binding energy of Ti $2p_{3/2}$ level in RT specimen is shifted toward to the lower energy than that of $CaTiO_3$. These results indicate that the outermost surfaces in H1 and H2 specimens include the $CaTiO_3$ state. On the other hand, the outermost surface in RT specimen does not include $CaTiO_3$ state and consists of some Ca and Ti oxide states.

The results of quantitative calculation from the integrated intensities are summarized in Table 4. If the outermost surface consists of stoichiometric $CaTiO_3$, the concentration (at%) of Ti should be equal to that of Ca. The concentrations of Ti and Ca are close together in H1 specimen. On the other hand, the concentration of Ti is smaller than that of Ca in H2. These results indicate that the outermost surface in H1 specimen consists of mainly stoichiometric CaTiO, whereas that in H2 specimen include less stoichiometric $CaTiO_3$. In addition, the increase of

Table 3 Binding energies of Ca $2p_{3/2}$, Ti $2p_{3/2}$ and O1s peaks obtained from $CaTiO_3$ thin films, CaO, $CaTiO_3$, and TiO_2 using XPS. Binding energy values were corrected by using Au $4f_{7/2}$ = 84.0 eV

Specimen	Ca $2p_{3/2}$ (eV)	Ti $2p_{3/2}$ (eV)	O 1s $[OH^-]$ (eV)	O1s $[O^{2-}]$ (eV)	Reference
RT	346.8	457.9	531.5	529.5	Present work
H1	346.6	458.6	531.8	529.7	Present work
H2	346.6	458.6	531.6	529.8	Present work
$CaTiO_3$	346.6	458.4	–	–	[8]
TiO_2	–	458.8	–	–	[8]
CaO	347.2	–	–	–	[8]

Table 4 Results of quantitative calculation from the integrated intensities obtained by using XPS. [X] means concentration (at%) of the X

Specimens	$\frac{[Ca]}{([Ca]+[Ti]+[O])}$	$\frac{[Ti]}{([Ca]+[Ti]+[O])}$	$\frac{[O]}{([Ca]+[Ti]+[O])}$	$\frac{[Ti]}{[Ca]+[Ti]}$
RT	0.18	0.11	0.71	0.37
H1	0.17	0.14	0.69	0.45
H2	0.20	0.12	0.68	0.38

concentration (at%) ratio of $\{[O^{2-}]/([OH^-] + [H_2O])\}$ in H1 specimen compared with that in H2 specimen will be resulted from less hydrated surface of H1 specimen.

SEM observation of specimen surface after immersion

Since $CaTiO_3$ film in RT specimen was not crystallized and dissolved abruptly, immersion test was not performed. Figure 3 shows the SEM image of the surfaces of specimens after 30- and 60-d immersions. After immersion for 30 d (Figs. 3(a) and 3(b)), the island-like precipitates were observed on the H1 specimen. After immersion for 60 d (Figs. 3(c) and 3(d)), the surface of specimen was completely covered with precipitate layer and large size precipitates initially observed on the specimens for 30 d disappeared. The precipitate layer contained cracks in Fig. 3(d). The cracks are caused by evacuation of the water in the layer in vacuo. Figure 4 shows the EPMA-EDX spectra of precipitates observed in SEM images after 30- and 60-d immersion (Fig. 3(b) and (d)). Only the peaks from Ca and P were observed, and these precipitates were asssumed as calcium phosphates. The inserted values of [Ca]/[P] correspond to atomic ratios of the calcium phosphate determined by the EPMA-WDS. After immersion for 30 d (Fig. 4(a)), the [Ca]/[P] ratio is slightly smaller than that of HAP {[Ca]/[P] = 1.67}. After immersion for 60 d (Fig. 4(b)), the [Ca]/[P] ratio of the layer is 1.67, and this value is the same as that of HAP. In the initial stage of HAP formation, calcium phosphate with a low {[Ca]/[P]} ratio is formed. The ratio increases with time scale of days and eventually approached to that of HAP. This phenomenon was explained by a faster adsorption of phosphate ions than that of calcium ions, the adsorbed phosphate ions give negative charges at the surface and attract passively charged calcium ions [15]. Our results can be explained by essentially the same mechanism.

Figure 5 shows the SEM image of H2 specimen surface after immersion for 60 d. The surface of H2 specimen was also covered with precipitate layer. Figure 6 shows the EPMA-EDX spectrum of precipitate layer. Not only Ca and P peaks but also Ti peaks are observed in the spectrum. Ti peaks are originated from the $CaTiO_3$ film and Ti substrate because the precipitate layer is thinner than the effective depth of

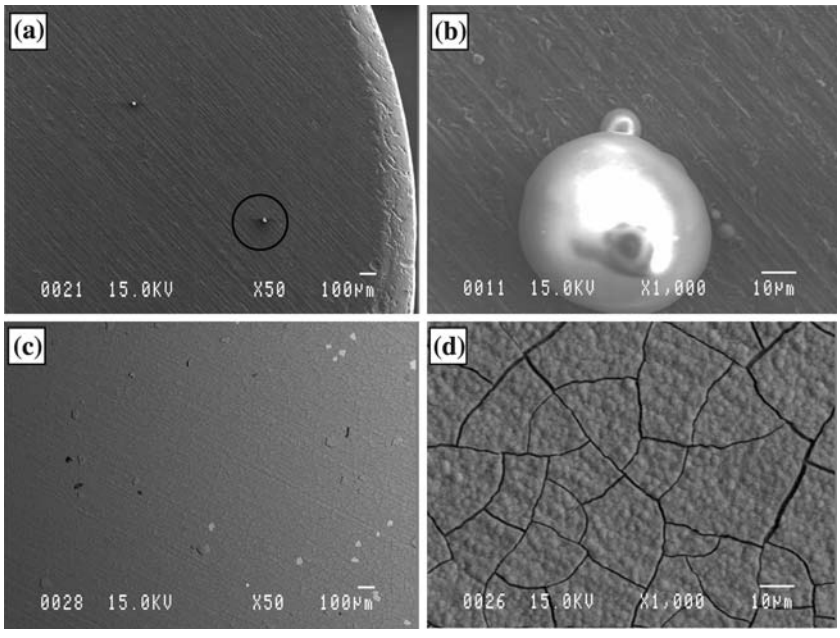

Fig. 3 SEM images of surface of H1 specimen after immersion in HBSS for 30 d (**a** and **b**) and after immersion in HBSS for 60 d (**c** and **d**)

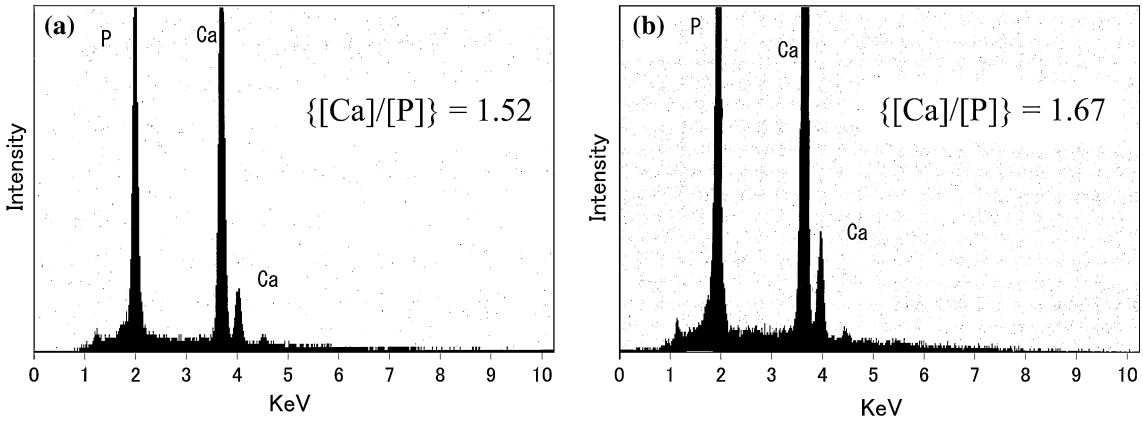

Fig. 4 EPMA-EDX spectra of precipitates of H1 specimen after immersion for 30 d (**a**) and after immersion for 60 d (**b**) in HBSS. Inserted {[Ca]/[P]} values correspond to atomic ratios of the precipitates determined by EPMA-WDS

Fig. 5 SEM images of surface of H2 specimen after immersion in HBSS for 60 d

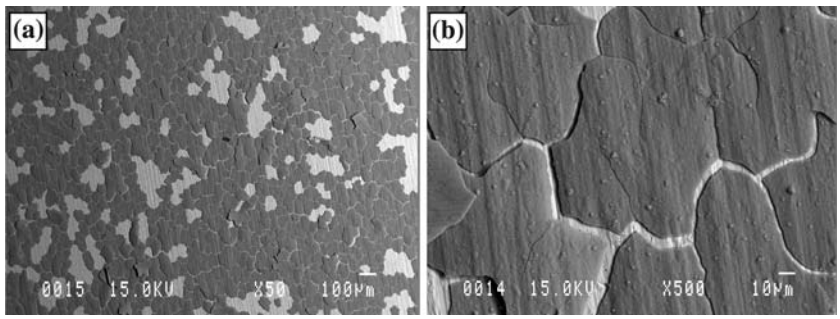

EPMA analysis. Thus, the precipitate layer is identified as calcium phosphates. The atomic ratio of {[Ca]/[P]} determined by the EPMA-WDS is also inserted in Fig. 6. The {[Ca]/[P]} ratio of the layer is slightly larger than that of HAP because Ca signal originated from the $CaTiO_3$ film is also included. The calcium phosphate layer on H2 specimen seems to be much easily peeled off from the substrate than that of H1 specimen. Furthermore, calcium phosphate was observed only on one of two H2 specimens shown in Fig. 5.

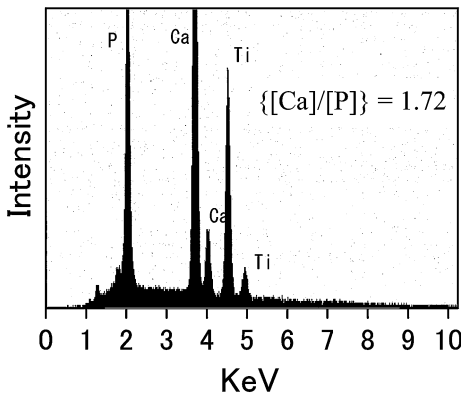

Fig. 6 EPMA-EDX spectrum of precipitates of H2 specimen after immersion for 60 d in HBSS. Inserted {[Ca]/[P]} values correspond to atomic ratios of the precipitates determined by EPMA-WDS

The results of SEM observation of all specimens are summarized in Table 5. The cpTi cannot form any calcium phosphate layer even after immersion for 60 d. Only H1 specimens can form calcium phosphate after immersion for 30, 45 and 60 d. Thus, H1 specimens showed the most stable growth of calcium phosphate layer. These results show that $CaTiO_3$ deposited 50 nm in thickness is enough to enhance the formation of calcium phosphates.

Table 5 The number of specimens formed calcium phosphate after immersion in HBSS

Specimens	30 d	45 d	60 d
cpTi	0/1	0/2	0/2
H1	1/1	2/2	2/2
H2	0/1	0/2	1/2

The number/number of specimen

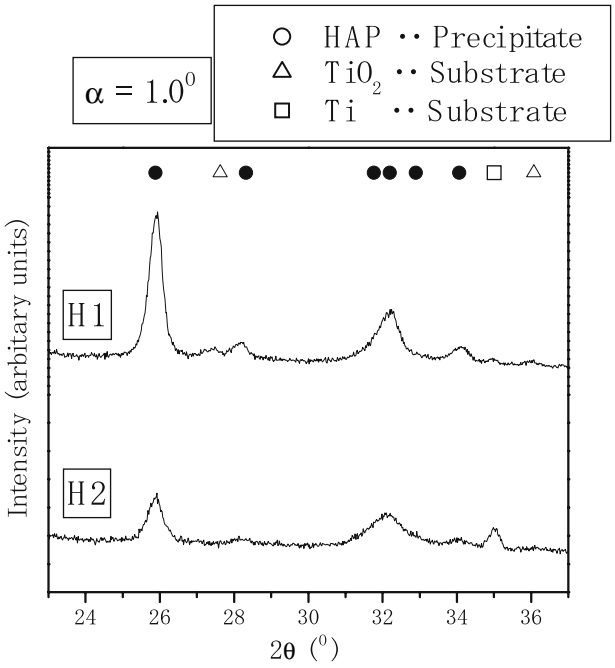

Fig. 7 GI-XRD patterns of the surface of H1 and H2 specimens after immersion in HBSS for 60 d

Figure 7 shows GI-XRD patterns of the surfaces of specimen H1 and H2 specimens after immersion for 60 d. The main peaks are assigned to reflection from HAP. Therefore, the calcium phosphate layers formed after immersion are identified as the HAP layers.

Thickness of calcium phosphate layer after immersion for 60 d

For estimating the thickness of the calcium phosphate layers formed after immersion for 60 d, the cross section of immersed specimens was observed by using SEM. Figure 8 shows the SEM images of cross section of specimens. The calcium phosphate layer on H2 specimen is very easily exfoliated from the substrate. On the other hand, it is rather strongly combined with the substrate on H1 specimen. The thicknesses of calcium phosphate layers determined from the SEM images are summarized in Table 6. The thickness of the calcium phosphate layer formed on the H1 specimen is four times as thick as that on H2 specimen. Thus, the growth rate of calcium phosphate layer on the H1 specimen is also faster than that of the H2 specimen.

Table 6 The thickness of the calcium phosphate layer formed after immersion in HBSS

Specimen	Thickness of calcium phosphate layer (μm)
H1	4.5
H2	1.2

Properties of $CaTiO_3$ film which is required to enhance calcium phosphate formation

Figures 3 and 4 show that the $CaTiO_3$ thin films of both H1 and H2 specimens can enhance the formation of calcium phosphates on Ti substrate. However, Tables 5 and 6 reveal that HAP film growth rates is large on H1 specimen. On both specimens H1 and H2, deposited $CaTiO_3$ is crystallized to perovskite-type $CaTiO_3$ and the compositions are similar. Differences are concentration of [OH] and [Ca]/[Ti] rate at the outermost surface of the deposited film.

Dissolution of Ca from the surface of materials is one of the important events for calcium phosphate formation in SBF. We consider that chemical stability at the outermost surface concern with the degradability of the film. We also attribute the high dissolution rate of Ca in H2 specimen than that in H1 specimen to the difference in the chemical stability of the outermost surface. The difference in the performance of calcium phosphate formation in H1 and H2 specimens may be caused by the difference in dissolution behavior of the outermost surface of the modified $CaTiO_3$ film deposited on Ti. However, more investigation in detail, e.g. determination of Ca amount dissolved into HBSS, is necessary to clarify this idea.

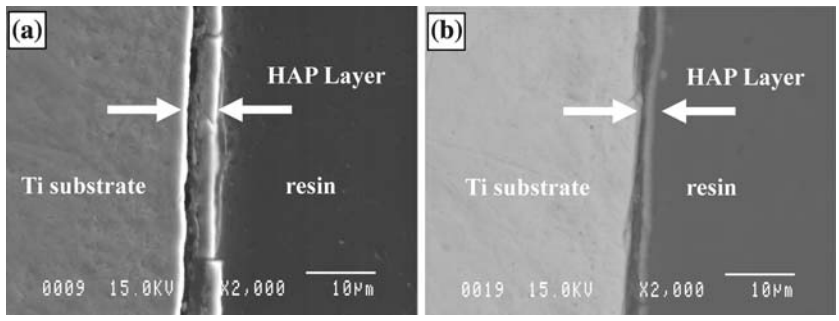

Fig. 8 SEM images of the cross section of: (**a**) H1 specimen and (**b**) H2 specimen after immersion in HBSS for 60 d

Summary

Deposition of $CaTiO_3$ at room temperature followed by annealing at 873 K in air or deposition at 873 K in vacuo could prepare the crystallized pervskite-type $CaTiO_3$ film on Ti. The outermost surfaces in both films were composed of $CaTiO_3$, whereas extent of convolution of hydroxides and other species than $CaTiO_3$ is high on the specimen deposited at 873 K and exposed to air.

After immersion in HBSS, formation of calcium phosphate was observed on $CaTiO_3$ film in both the $CaTiO_3$ film annealed in air and the $CaTiO_3$ film deposited at 873 K. The {[Ca]/[P]} ratio of the calcium phosphate formed on $CaTiO_3$ film at the initial stage is slightly smaller than that of hydroxyapatite. The ratios increased with immersion time and finally reached that of hydroxyapatite. In addition, when calcium phosphate layer was sufficiently thick, it was crystallized to hydroxyapatite. These results indicate that crystallized $CaTiO_3$ film with thickness of 50 nm can enhance the calcium phosphate formation. However, growth rate of the calcium phosphate layer is high on the specimen where the $CaTiO_3$ film was annealed in air in comparison with $CaTiO_3$ film deposited at 873 K. Therefore, in order to enhance the calcium phosphate formation efficiently, $CaTiO_3$ film should be modified by annealing in air rather than deposition on heated substrate in vacuo.

Acknowledgment The authors thank Mr. Yoshihiro Murakami for operating the EPMA.

References

1. A. YAMAMOTO, R. HONMA and M. SUMITA, *J. Biomed. Mater. Res.* **39** (1998) 331
2. M. PAPAKYRIACOU, H. MAYER, C. PYPEN, H. PLENK Jr and S. STANZ-TSCHEGG, *Int. J. Fatigue* **22** (2000) 873
3. K. YaMashita, E. YONEHARA, X. DING, M. NAGAI, T. UMEGAKI and M. MATSUDA, *Biomed. Mater. Res.* **43** (1998) 46
4. K. van DIJK, H. G. SCHAEKEN, J. G. G. WOLKE and J. A. JANSE, *Biomaterials* **17** (1996) 405
5. C. K. WANG, J. H. CHEN LIN, C. P. JU, H. C. ONG and R. P. H. CHANG, *Biomaterials* **18** (1997) 1331
6. K. A. KHOR, Y. W. GU, C. H. QUEK and P. CHEANG, *Surf. Coat. Tech.* **168** (2003) 195
7. T. HANAWA, Y. KAMIURA, S. YAMAMOTO, T. KOHGO, A. AMEMIYA, H. UKAI, K. MURAKAMI and K. ASAOKA, *J. Biomed. Mater. Res.* **36** (1997) 131
8. T. HANAWA, H. UKAI and K. MURAKAMI, *J. Electron Specctrosc. Relat. Phenom.* **63** (1993) 347
9. D. KRUPA, J. BASZKIEWICZ, J. A KOZUBOWSKI, A. BARCZ, J. W. SOBCZAK, A. BILINSKI, M. LEWANDOWSKA-SZUMIEL and B. RAJCHEL, *Biomaterials* **22** (2001) 2139
10. N. OHTSU, K. SATO, K. SAITO, T. HANAWA and K. ASAMI, *Mater. Trans.* **45** (2004) 1778
11. J. H. SCOFIELD, *J. Electron Spectrosc. Relat. Phenom.* **8** (1973) 129
12. N. OHTSU, T. ASHINO and K. ASAMI, *Mater. Trans.* **45** (2004) 550
13. S. KACIULIS, G. MATTOGNO, A. NAPOLI, E. BEMPORAD, F. FERRARI, A. MONTENERO and G. GNAPPI, *J. Electron Spectrosc.* **95** (1998) 61
14. P. A. W. van der HEIDE, *Surf. Sci.* **490** (2001) L619
15. M. UCHIDA, H. M. KIM, F. MIYAJI, T. NAKAMURA and T. KOKUBO, *J. Am. Ceram. Soc.* **84** (2001) 2041